No. 2569

EXPERIMENTAL AND NUMERICAL STUDY OF AIR MOVEMENT IN SLOT-VENTILATED ENCLOSURES

DR. MICHAEL B. TIMMONS, P.E. **DR. LOUIS D. ALBRIGHT**
Associate Member ASHRAE

DR. RONALD B. FURRY **DR. KENNETH E. TORRANCE**

ABSTRACT

Air flow patterns were studied for rectangular enclosures ventilated by a planar jet issuing from a slotted inlet. Experiments showed that:

1. Flow patterns are independent of Reynolds number above a threshold value (approx. 3,800);
2. The coanda effect and attachment length of the jet are affected by inlet and outlet diameter, length of flow, and distance to the nearest wall;
3. Some geometries result in bistable flows.

In order to explain the experiments and obtain predictive relations thereof, a numerical model was developed. Using the assumption of inviscidness, a functional relationship between vorticity and stream function was established to express the vorticity equation as a Poisson Equation, $\nabla^2\psi = f(\psi)$.

The experimental findings and established jet theory for turbulent jets were the basis for determining the functional relations. Comparisons between experimental and numerical results showed the model can be used to predict flow patterns and velocity fields in slot-ventilated enclosures.

INTRODUCTION

The importance of ventilation is most evident when the ventilation system is malfunctioning. Excessive levels of heat, cold, air movement, or noxious gases within ventilation enclosures for humans or animals usually identify a malfunctioning ventilation system. A less than optimum environment in the ventilation enclosure leads directly to a less efficient performance by the occupants. Often the problem can be directly traced to the air distribution system. Although there are handbooks for designing the supply system and the required amount of fresh air (ASAE Yearbook [1] and the ASHRAE Handbook [2]) the engineer/architect usually resorts to rule-of-thumb methods to design the distribution system. What is needed is a simple tool to aid designers to predict air flow patterns and velocities within an enclosure prior to installation of the ventilation system.

The inherent difficulty in developing a predictive method has been the complexity of the problem itself - a turbulent fluid flow. Predictive methods to date have required solution of the full Navier-Stokes Equations with some form of statistical decomposition used to account for the randomness of the turbulent motion. The origins of such methods lie with Reynolds [3], Taylor [4] and Von Karman [5]. The advent and rapid development of the digital computer has allowed the original analytical methods to be expanded (Launder and Spalding [6] and Lumley [7]).

M.B. Timmons is Assistant Professor, Department of Biological and Agricultural Engineering, N.C. State University, Raleigh; L. D. Albright is Associate Professor, Department of Agricultural Engineering, Cornell University; R. B. Furry is Professor, Department of Agricultural Engineering, Cornell University; K. E. Torrance is Associate Professor, Sibley School of Mechanical and Aerospace Engineering, Cornell University.

air. This assumption is based on the premise that under such a condition, a small amount of condensation occurring over a brief cold period will be either evaporated or sublimated during warm periods, thereby precluding an accumulation of moisture on the underside of the roof sheathing.

It is difficult to include the effect of storage of moisture on the underside roof surface in a time-dependent model because relations for the transient diffusional flow of water vapor through the ceiling and other surfaces of the attic have not yet been formulated in the literature.

A strong need exists to verify experimentally the mathematical model and to investigate the effect of storage of moisture on the required attic ventilation rates.

G.H. GREEN, Prof., Univ. of Sask., Saskatoon, Sask.: What was the relative humidity of both the humidified house and the non-humidified house?

BURCH: The indoor relative humidity levels used for the analysis are given in Table 6 of the paper. The relative humidity levels without humidification are based on values for an average house given in Fig. 5 of Chapter 20 of the ASHRAE HANDBOOK OF FUNDAMENTALS.[4] Values for a humidified house are based on the limiting indoor relative humidity for double-pane glass given in Table 1 of Chapter 5 of the ASHRAE EQUIPMENT HANDBOOK.[13]

GREEN: Photographic evidence of frost buildup in attics shows much of the frost accumulation is in the insulation above the openings at light fixtures, etc. Please comment since your model only considers frost accumulation on the roof.

BURCH: I believe that condensation will occur at the coldest surfaces of an attic. Radiation exchange between a roof and a clear winter night sky substantially reduces the exterior surface temperature of a roof. Under a still air condition, the reduction in surface temperature below the outdoor air temperature can be as much as 20 F. Under such a situation, it would seem that the underside roof surface would be the coldest part of an attic and would therefore be the part most susceptable to condensation.

DAVID T. HARRJE, Sr. Resch. Engr., Center for Energy & Envir. Studies, Princeton Univ., Princeton, NJ: The fraction of exfiltration air moving through the attic based upon our studies in wood-frame houses in the Northeast is at least equal to your estimate of 20%. Thus, we view the 20% value as a reasonable estimate.

E.A. SCOTT, Commercial/Industrial Mgr., Mcgraw-Edison, Phoenix, AZ: Has, or will, a committee address the attic ventilation rates applicable when evaporative cooling is vented through the attic space? Other considerations include: air change rates, condensation potential, temperature barrier effectiveness.

BURCH: The present paper does not cover the application of evaporative cooling vented through an attic spare.

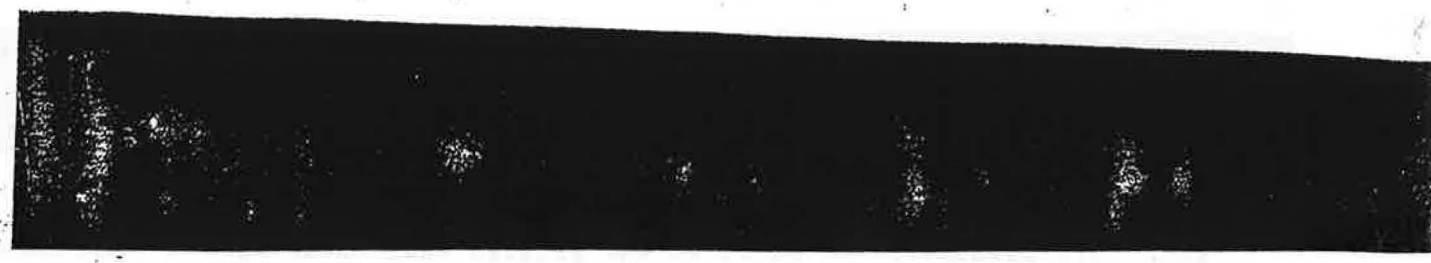

However, such methods are becoming increasingly complicated and therefore do not address in a practical manner what the designer's primary interest is: flow patterns and velocities to be expected within a ventilated enclosure.

OBJECTIVES

(a) Develop a simple, numerical model capable of predicting the flow patterns and velocities in slot-ventilated enclosures, and

(b) Evaluate the model by direct comparison to experimental results.

EXPERIMENTAL INVESTIGATION

Numerical simulation and predictions based upon models which have not been tested against experimental data are not useful. Therefore, the numerical model was compared to data obtained from a physical prototype. In designing the physical prototype, one goal was established to guide its design: the prototype should be simple in geometry and flow characteristics and still retain physical simplicity.

Further design considerations were mandated by the requirement that the flow remain turbulent. Parczewski [8] and Reinmann [9] have both shown that for turbulent flows: (1) flow patterns are independent of changes in the Reynolds Numbers, and (2) where equal fluid velocities are established in model and prototype, identical velocities should exist at scaled locations in the model and prototype. Such an attribute of turbulent flow allows data obtained from an experimental model to be directly applicable to other enclosures of similar geometry.

Experimental Equipment

A wind tunnel was constructed with the test section representing a ventilated enclosure. The geometry of the test section could be varied and a damper on the ventilating fan allowed Reynolds numbers* to be changed.

An abrupt inlet contraction plenum was installed which changed the inlet area from 900 mm x 1500 mm to 50 mm x 1000 mm to minimize the turbulence level where the jet first entered the test section. Lumley [10] showed that turbulence intensity decreases by the square of the contraction ratio (c^2) for fluctuations aligned with the tunnel axis, and by the square root, $c^{1/2}$, for fluctuations normal to the tunnel axis, where c is the contraction ratio. Six layers of window screening, 0.3 mm wire diameter and 3 x 2 strands per cm^2, were placed at the beginning of the contraction to reduce further turbulence present in the laboratory. Dryden and Shubauer [11] give predictive relationship for turbulence reduction due to the installation of filtering screens:

$$\text{reduction factor} = 1./(1+k)^{1/2} \qquad (1)$$

Variables are defined in the list of symbols.

A 2-dimensional jet at the inlet was obtained for the test section using a 20 to 1 slot length to width ratio which was found by Foerthmann [12] to produce a 2-dimensional jet. Using a chamber depth of 1000 mm required the slot width to be 50 mm or less. The chamber's dimensions were established as: depth, 1000 mm; cross section, 500 mm x 1000 mm; inlet slot width, 50 mm; and outlet slot width, 100 m. A false end wall containing the slotted outlet was used to vary the flow length. The inlet plenum was movable, which allowed different inlet placements.

A fan was selected that would supply the required flow rates to maintain the range of Reynolds numbers to be used for the study. For instance, a Reynolds Number of 5,500 required a flow rate of 0.055 m^3/s.

The exhaust plenum retained the cross-sectional area and shape of the outlet (100 x 1,000 mm) for the first 500 mm downstream to minimize any effect the exhaust plenum would have on the internal flow of the chamber. The wind tunnel with entrance and exhaust plenums is shown in Fig. 1.

---

*Reynolds numbers are always based on inlet velocity and slot width.

The plane of the photograph is the "z" coordinate, and air flow through the tunnel is in the x direction. The 2-dimensional flow in the test section is considered to be in the xy plane. (See Fig. 6.)

Air flow patterns were made visible using a Sage Action, Model 33 bubble generator and a 150 W Xenon arc lamp to provide a plane of light (approx. 80 mm thick) to illuminate bubbles such that a photograph could be obtained to show the 2-dimensional flow inside the chamber. The bubbles were introduced at the rear of the inlet contraction downstream from the filtering screens. The neutrally buoyant bubbles were produced at a rate of approx. 400/sec and were approx. 3 mm in diameter.

Mean velocities, converted from rms voltage recordings, were obtained with a hot wire anemometer. The probe tip used was a metal clad sensor. The tip was calibrated and the voltage output linearized for the range of velocities expected in the experiments.

The wind tunnel was designed to provide a 2-dimensional flow in the test section. Inlet and outlet velocity transverses plus photographs of the air flow patterns were taken at the 1/4, 1/2 and 3/4* planes of the test section. Velocity profiles were within a 2% variation among the planes and inspection of the photographs did not reveal any significant differences between the planes (see Timmons [13] for photographs).

Unforeseen effects of the laboratory or geometric idiosyncrasies of the wind tunnel were investigated by locating the inlet slot in mirror symmetric locations. Inspection of the subsequent flow patterns did not reveal any significant difference. It was concluded that the chamber was constructed to be capable of providing consistent results to which predictions of the numerical model could be compared.

Independence of flow patterns to changes in Reynolds number above a threshold limit was also established. Inspection of Fig. 2 demonstrates that no significant differences occur in the flow patterns, flow separation or jet attachment for the three Reynolds numbers studied: 3800, 5500, and 11,000. It was, therefore, concluded that the flow patterns obtained above a threshold Reynolds Number of 3,800 were independent of the Reynolds Number.

NUMERICAL MODEL

The numerical model developed in this paper is a kinematic relationship, the vorticity equation

$$\nabla^2 \Psi = -\omega \tag{2}$$

in which the dynamics of the fluid flow are modelled. The primary assumption used in the model is inviscidness, such that the vorticity transport equation for a 2-dimensional flow (Roche [14])

$$\frac{D\omega}{Dt} = \nu\nabla^2\omega \tag{3}$$

can simply be written as a material derivative.

$$\frac{D\omega}{Dt} = 0 \tag{4}$$

As a result of the inviscid assumption, vorticity can be neither created nor destroyed throughout the fluid. The vorticity, or vortex lines, are said to move with the fluid, which is equivalent to maintaining the values of vorticity constant along streamlines. Similarly, a constant value of stream function, Ψ, also corresponds to a streamline. Therefore, it follows that a value Ψ also corresponds to a streamline. Therefore it follows that a value ψuniquely establishes a value of vorticity. That is,

$$\omega = f(\psi) \tag{5}$$

as a result Eq 2 may be rewritten as

$$\nabla^2\psi = f(\psi) \tag{6}$$

*1/4, 1/2 and 3/4 planes are in the xy orientation and are 250 mm, 500 mm, and 750 mm from the bottom (z = 0) of the test section.

Some confusion may result from referring to the model as an inviscid model. The model development is based upon relationships derived from jet theory for jet entrainment, jet expansion, and jet vorticity. All of these phenomena are obviously affected by or occur partly or wholly due to viscosity. However, the essential idea of the model is to determine the relationship between vorticity and stream function and use the vorticity equation, Eq 2, to predict the fluid flow.

Since an inviscid model does not destroy or create vorticity, in effect the model attempts only to determine how the vorticity which enters the flow from the inlet is redistributed. Therefore, it is only the effects of the vorticity introduced at the inlet which were modelled. Vorticity which is produced by flow separation caused by obstructions within the enclosure must be separately modelled, since all surfaces are assumed to be perfect slip walls due to inviscidness.

Formulation of the Numerical Model

The development of the numerical model can be summarized as the determination of the functional relationship between vorticity and stream function as shown in Eq 5. The model development follows the scheme given below and will be followed by its formulation:

1. The maximum vorticity in the jet is calculated from
   (a) the data of Abramovich [15] to estimate jet centerline velocity, u_{jet},
   (b) a kinematic relation to estimate tangential velocity of the eddy, u_e, and
   (c) divergence data for free jets (Abramovich [15] to estimate the average mixing layer thickness, Δy;
2. The vorticity profile is calculated from the velocity profile for a free jet as given by Albertson [16];
3. The vorticity in the standing eddies is determined by relating the tangential velocity of the eddies to the vorticity profile of a free jet;
4. Vorticity is expressed as a function of stream function.

Maximum Vorticity in the Jet. The vorticity in a 2-dimensional flow is (Sabersky [17])

$$\omega = \frac{\partial v}{\partial x} - \frac{\partial u}{\partial y} \tag{7}$$

In a free jet, Eq 7 can be approximated as follows:

$$\omega_{jet} = \frac{\partial u}{\partial y} \approx \frac{\Delta u}{\Delta y} = \frac{u_{jet} - u_e}{b} \tag{8}$$

If Δu and Δy can be obtained in Eq 8, the maximum vorticity of the jet may also be approximated.

If Δy is defined as the distance b from the centerline to the outside edge of the jet, it it follows that Δu is the difference between the velocity at the centerline, u_{jet}, and the velocity at the edge of the jet, which is the tangential velocity of the standing eddy above or below the jet. Obviously if there are no standing eddies, the velocities at the edges of the jet are zero.

The velocity at the centerline of the jet is a function of the distance the jet has traveled. A general approximation used in the model is that for variables which vary with the distance traveled, (e.g., width of the jet or velocities in the jet) the average value for the variable from the inlet to the outlet will be used everywhere along the jet's length. For example, the centerline jet velocity is calculated as the average of the velocity at x = 0, and x = L. Abramovich (Ref 15, p. 509) presents a graph showing the variation of jet velocity with distance. His data were used to estimate jet decay.

The second component of Δu is the maximum tangential velocity of the standing eddy above or below the jet. Maximum tangential velocity of a standing eddy is

$$u_e = u_{jet} (1 - \sigma) \tag{9}$$

Appendix A gives the proof. For cases in which the tangential velocity is different in the two eddies, the average tangential velocity is used in calculating Δu. Using the average tangential velocity to estimate vorticity in the jet results in equal magnitudes of the vorticity above and below the centerline of the jet.

The calculation of Δy assumes that the enclosure walls will not affect the spread of the jet. Abramovich [15] presents divergence angles for jets as 9 deg and 12 deg, 30 min. for the initial and main regions of the jets. There is also a region of transition between the initial and main region of the jet flow. In this paper it is assumed that the length of the transition region is zero. Again, this approximation is not critical to the development of the model since the estimate of the half width of the jet does not significantly change if a transition region is included.

Abramovich [15] estimates the length of the initial region of the jet, X_H, as between 3 to 4-1/2 inlet diameters depending upon the characteristics of the inlet profile. The average mixing layer thickness, Δy, can then be estimated as 1/2 of the mixing layer thickness at $X = L^*$.

$$\Delta y = 1/2b = 1/2\{X_H \tan 9° + (L - X_H) \tan 12° 30' + b_o\} \tag{10}$$

Vorticity Profile of a Free Jet. Since vorticity is to be made a function of ψ across the entire flow (i.e., across and beyond the edges of the jet), an algebraic relationship is needed to make vorticity a function of y (y is later expressed in terms of ψ). With such a relationship, a value of vorticity may be assigned for any stream function value. The vorticity profile is obtained by differentiating the velocity profile for a free jet and imposing the calculated vorticity levels of the standing eddies on the vorticity profile of a free jet (see Fig. 3).

Abramovich (Ref 15, p. 180) gives the following equation for the velocity profile in the main region of a free jet

$$\frac{\Delta V}{\Delta V_m} = \{1 - (y)^{1.5}\}^2 \tag{11}$$

where y in this instance is made dimensionless based on the local 1/2 width of the jet, b. The origin for y is the centerline of the jet and is positive in the gravitational direction (opposite from normal convention). Eq 11 agrees well with profiles measured in free jets by Foerthmann [12] and Albertson [16]. The ΔV in Eq 11 accounts for possible non-zero values of the velocities of external streams at the edges of the jet.

A vorticity profile of a free jet can be obtained by differentiating Eq 11 with respect to y, resulting in a profile with a maximum magnitude of 1.42. The preceeding profile is divided by 1.42 to give a profile such that the maximum vorticity becomes unity.

$$\omega(y) = \{(-3y^{0.5} + 3y^2)/1.42\} \ \omega_{jet} \tag{12}$$

The vorticity profile given by Eq 12 (a maximum vorticity of one) can then be used to provide the vorticity profile of a jet in which the maximum vorticity is defined by Eq 8.

For an enclosed flow, the vorticity profile, Eq 11 is complicated by the presence of rotational flow above and below the jet where fluid is entrained and recirculated in the enclosure. These rotating areas, known as standing eddies, have a uniform level of vorticity (Squire [18]). The numerical model is formed assuming that the values of vorticity in the standing eddies are imposed upon the vorticity profile of the free jet. The vorticity profile is approximated in the model by straight lines between the break points of the vorticity profile and the vorticity values in the standing eddies (see Fig. 3). The method of assigning values of vorticities in standing eddies must next be estimated.

Magnitude of Vorticity in Standing Eddies. The key to the development of the entire numerical model was the manner in which the vorticity was assigned to the standing eddies. The method developed used the tangential velocity of the standing eddy(s) found from Eq 9 to establish the y value, y_e, on the dimensionless velocity profile for a free jet, Eq 11, and then substituting y_e into Eq 12. The resulting vorticity value is multiplied by the maximum jet vorticity to give

*All variables are always expressed in dimensionless form using characteristic variables of inlet width and inlet jet velocity, unless otherwise noted.

the uniform value of vorticity, ω_e, in the standing eddies. The steps to determine ω_e are restated for convenience:

1. Eq 11 is used to calculate y_e, letting ΔV be the tangential velocity of the eddies, u_e;
2. y_e is substituted into Eq 12 to calculate ω_e;
3. Since Eq 12 is for a maximum vorticity of unity, ω_e is adjusted based upon the maximum magnitude of vorticity in the jet found from Eq 8.

Expressing Vorticity as a Function of Stream Function. Since the objective of the model development is to solve the vorticity equation in Poisson's form, Eq 6, the vorticity profile for the jet and standing eddies must be expressed as a function of ψ and not y. While the jet edges are always defined by ± 1, the ψ values increase from their normal values* of one and zero to values above one and less than zero due to fluid entainment into the jet. The mass flow in the jet as a function of X can be determined from an entrainment relation as given by Albertson [16]:

$$\frac{Q}{Q_o} = 1. + 0.080 \frac{X}{2b_o} \tag{13}$$

Remembering that flow in a jet is also defined by $\Delta\psi$ from the top to the bottom of the jet, the average amount of fluid entrained into the jet from X = 0 to L is (using Eq 13 at X = L)

$$\overline{\Delta\psi} = 1/2\ \Delta\psi = 1/2\ \Delta Q = 1/2\ \left\{\left(Q_o + 0.080 \frac{L}{2b_o}\ Q_o\right) - Q_o\right\} \tag{14}$$

Finally, the average stream function values from X = 0 to L at the jet edges, assuming equal entrainment into the top and bottom of the jet, are

$$\psi_{jet} = 0.5 - \left(0.5 + \frac{\overline{\Delta\psi}}{2}\right)y \tag{15}$$

From Fig 3, it is seen that 5 values of stream function are needed to describe the distribution of vorticity. The 5 points are determined as follows:

1. Vorticity maxima are found by differentiating the vorticity profile with respect to y and setting the result to zero. The results are maximum at $y = \pm 0.4$;
2. The centerline of the jet is defined by y = 0;
3. The y values for the points at which the eddy vorticity joins the free profile of vorticity are determined from Eq 11.

Substituting these 5 values of y separately into Eq 15 allows the profile for vorticity to be obtained, which is used in the numerical model. An approximation is made in Eq 15 by assuming uniform flow in the jet. That is, ψ varies linearly with y. A correction could be applied to Eq 15 to account for nonuniform jet flow between y_1 and y_5.

Numerical Method and Computational Scheme

A relationship has now been established between vorticity and the stream function so that the vorticity equation can be solved in the form shown in Eq 6 where f is now known. Eq 6 may be solved iteratively using a Successive Over Relaxation scheme, which is thoroughly discussed by Roache [14]. Sweeps through the field are alternated in the y direction, but always in the increasing x direction. After each iteration of the field, the vorticity at each grid point is updated based upon the newly calculated stream function value at the point. The calculation is considered to have converged when the change in stream function at the centerpoint of the calculation (x equal to L/2 and y equal to H/2) is less than a prescribed tolerance, ε. For the calculations in this paper, ε was set at 0.005. Convergence checks for the model using uniform grids of 11 x 11, 21 x 21, and 31 x 31** were also performed which showed a grid spacing of 21 x 21 to be more than adequate for resolution of the vorticity equation.

---

*Boundary values of stream function as chosen such that mass flow through the enclosure is one unit.

**Convergence was checked for a geometry of H = L, $D_1 = D_2$ and D_1 = 3/10 H. See Fig. 6 for variable identification.

The choice of initial conditions was also shown not to influence the convergent solutions. Preliminary models which established vorticity levels based solely on jet shear-layer thickness suffered the common characteristic of predicting flow fields which were dependent upon the initial choices of stream function values for the numerical field. However, the numerical model presented herein was shown to predict the same numerical field regardless of the initial choice of stream function field (see Timmons [13] for numerical results and a complete discussion). The key attribute of the successful model was that the vorticity distribution was related to the entire dimensionless jet profiles of velocity and vorticity.

A practical advantage of the numerical model* is its simplicity; only the vorticity equation is needed to describe the flow. As a result, the computation time required for a solution on a digital computer is fairly short when compared to the computation times required to solve the full (or decomposed) Navier Stokes equation. The computation times for the numerical model presented in this paper using an IBM 370-168 were in the 15 to 30 sec range for a 21 x 21 mesh and a convergence criterion of 0.0005.

NUMERICAL AND EXPERIMENTAL RESULTS

The adequacy of the numerical model was established by comparison to experimental results for flow patterns and velocity fields. A direct comparison between predicted and measured flow patterns and velocity traverses is given in Fig. 4 and Fig. 5 for the geometry specified in Table 1 as Test 1. Fig. 6 depicts the geometric variables for specifying the enclosure test conditions. The steam function plot, Fig. 4, was obtained from the numerical fields given in Table 2. The streamlines are actually bands about a prescribed value of the stream function. All plots divide the maximum range of ψ into 10 divisions. The plot routine also was written to change symbol plots whenever the ψ changed sign or increased above $\psi = 1.0$. In this manner the edges of the jet mass core can be more easily identified in the plots. However, to determine the edges of the mass core accurately, the ψ fields should be consulted.

Comparison of the predicted and photographed flow patterns shown in Fig. 4 show very close agreement in such features as the large dominant eddy above the jet and the attachment of the jet to the lower wall. Predicted velocities** were extracted from the stream function field by using forward difference approximations for u and v (see Roache [14]):

$$u_{i,j+1/2} = \frac{\partial \psi}{\partial y} = \frac{\psi_{i,j+1} - \psi_{i,j}}{\Delta y} \tag{16}$$

$$v_{i+1/2,j} = -\frac{\partial \psi}{\partial x} = \frac{\psi_{k,j} - \psi_{i+1,j}}{\Delta x} \tag{17}$$

The direct comparison of recorded and predicted velocities shown in Fig. 5 again shows reasonably close agreement. Discrepancies near solid walls will be discussed later.

Attachment Lengths and the Coanda Effect

The investigation and development of predictive relations of jet attachment have been previously investigated by Borque and Newman [19] and Sawyer [20]. Using the relation developed by Borque, an attachment length, ℓ_r, of 240 mm is predicted for the geometry of Test 1 shown in Table 1. The actual attachment length measured in Test 1 was 280 mm and the flow field obtained from the numerical model shows an attachment length of 310 mm (interpolated from stream function field). The geometry was changed from Test 1 such that the inlet was located in the center of the inlet wall resulting in an attachment length of 480 mm $\pm$ 40 mm (jet attachment point fluctuates). The relations derived experimentally by Borque and Newman predicts 506 mm. The experimental agreement with the results of Borque help to establish confidence in the chamber constructed for the present study, and the results obtained using it. The first comparison between the measured and predicted attachment length for Test 1 is also quite good considering the simplicity of the numerical model used.

The results obtained by Borque and Sawyer were from a flow with an unrestricted outlet, i.e., $D_2 = H$. Therefore it is questionable whether the predictive equations for jet attachment length developed by Borque and Sawyer are directly applicable to enclosed flows with a restricted outlet. The question was solved by experiments in which the geometry of Test 1

*For a listing of the computer program with sample inputs and outputs, see Timmons [13].

**A 41 x 41 grid was used, which required the velocities at 2 grid points to be averaged so that a direct comparison could be made for the locations at which the velocities were recorded.

(with inlet in two locations, i.e., b_1 = 100 mm or 225 mm) was altered by moving the outlet wall towards the inlet wall, thereby shortening L. It was found that the coanda effect disappears when the predicted attachment length, ℓ_r, is approximately equal to L as shown in the photographs of Fig. 7.

The numerical model was also shown to predict the same effect by using the geometries given in Table 1 as Test 2 and Test 3. The only difference between the two tests is that the length of flow, L, was increased from 500 mm to 1000 mm. The numerical results are shown in Figure 8 and the stream function fields are given in Tables 3 and 4. Inspection shows that the attachment length has decreased from 200 mm in Test 2 to approximately 0 mm in Test 3, which is the same type of effect shown in the photographs of Figure 8.

If the inlet is placed in the center of the wall for the geometry of Test 1 (B_1 changed to 225 mm), a bistable flow condition results in that the jet will attach to either the top or bottom wall. The numerical model was shown to be able to predict the same phenomenon if the vorticity in one of the standing eddies is increased or decreased by 5 to 10%. The perturbed level of eddy vorticity caused the jet to move away from the stronger eddy and attach to the opposite wall (if the D_1 to L ratio is small enough to allow the coanda effect to be present).

DISCUSSION

The development of the numerical model depended upon the assumption that the flows considered were inviscid. It is known that the viscous effects are inversely proportional to the Reynolds number (Tennekes (21)). Since turbulent flows require minimum Reynolds numbers of two to four thousand, the inviscid approximation is justified. However, in boundary layers near walls, the viscous effects are significant and, therefore, the inviscid approximation breaks down leading to errors in velocity predictions.

A comparison between the predicted and measured velocities for Test 1 shown in Figure 5 did reveal that the velocity predictions were in general too high near the solid walls. The error is primarily due to the inviscid approximation which allows free or perfect slip at the walls. Furthermore, the approximation of constant vorticity in the large recirculating eddy imposes solid body rotation for the eddy motion. Solid body rotation, i.e., the angular velocity is constant, requires the tangential velocity to increase linearly with the radius of the body as is predicted for the eddy. However, the close agreement shown between predicted and photographed flow patterns shown in Figure 4 suggests that errors in velocity predictions near the walls do not affect the accuracy of predicting flow patterns.

Vorticity Equilibrium of Standing Eddies

Part of the development of the numerical model was based upon the hypothesis that the equilibrium vorticity levels in the standing eddies are defined by the tangential velocities of the eddies. This hypothesis is supported by the accuracy of the results, and was developed primarily from experimental observation. Bubble traces clearly indicated that the dominant transfer of vorticity occurs across the mixing layers of the jet, especially during the initial period after the fan is turned on and the jet is initiated. It is believed though, that the final equilibrium levels of vorticity in the eddies are dictated by the magnitude of the vorticity transported by the masses of fluid which are shed from the jet and recirculated into the standing eddies. The velocity of the masses of fluid which are recirculated may be estimated in a first approximation as being the tangential velocity of the individual eddy. The tangential velocity can be used to infer the vorticity of the recirculated masses by using Eqs. 9 and 12. This method, which is related to the dymamics of the fluid motion, was the only method found which could be consistently applied to a variety of geometric conditions, and still give reasonable predictions of flow patterns and jet deflection (coanda effect).

Capabilities and Limitations

The numerical model has been shown to predict flow patterns which agree to a large extent with the flow patterns observed experimentally for the geometries considered in this study. The model was shown to be able to predict the coanda effect and to be consistent in its predictions of increasing or decreasing attachment lengths, l_r, by changing the lengths of the enclosure, L.

A limited set of geometries were simulated, however, and the question naturally arises as to the overall applicability of the model. More specifically, in all the geometries considered, the ratio of (L/D_1) was always relatively small compared to what can occur in some ventilated structures. As (L/D_1) increases, the jet velocity (physically speaking) continues to decay and spread, thus, weakening the vorticity. Eventually the velocity fluctuations due to turbulence become of comparable order to the jet velocities, which effectively ends the region of jet flow. The flow in such enclosures might be expected to contain one very large but weak eddy and have an identifiable jet in part of the flow. Alternately, the enclosure could show an area of potential flow beyond the location where the jet is said to have dissipated.

In the numerical model, regardless of the D_1/L ratio, a finite value of jet vorticity will exist. As a result the model will predict a flow pattern showing jet flow to the outlet with a large recirculating area above or below the jet. If the jet vorticity is made equal to zero, a potential flow pattern is predicted with no flow separation at the inlet. Thus, the behavior of the numerical model can be compared to fluid flows that are close to being inviscid, yet reveal flow patterns completely different from what a theoretical solution assuming inviscidness would suggest (see Tani [22]).

The only formal restriction on the use of the model developed in this paper is a Reynolds Number criterion. It was shown that above a given Reynolds Number, the flow patterns within the enclosure are independent of further increases in Reynolds Number. A Reynolds Number of 3,800 based on inlet jet velocity and slot width was found adequate to assure flow pattern independence to Reynolds Numbers. Therefore, in a slot-ventilated enclosure, a minimum Reynolds Number of 3,800 is also required if the model developed in this paper is to be applicable. Typical inlet velocities in slot ventilated barns are of order 5 m/s which would in turn require the slot width to be greater than 8 mm (using ν as 10^{-5} m^2/s). Common slot widths in agricultural buildings are 20 mm to 100 mm, which would imply that the model could be used to predict the air flow patterns in such buildings. Similar reasoning can be applied to other ventilated enclosures to determine the applicability of the method.

Finally, let it be restated that the model developed in this paper predicts flow patterns as the result of vorticity production at the inlet. For enclosures that have no internal obstructions, the agreement between predicted and observed flow patterns suggests that flow patterns are mainly a result of the vorticity produced in the inlet. If the inclusion of obstructions is desired, it is possible that the approach applied in this paper may also be used to model the vorticity production at the obstruction and its effect on the enclosure flow patterns. At least it is worthy of further pursuit. The alternative is to use the full dynamic equations and accept the associated computational complexity of such a set of equations.

CONCLUSIONS

From experimental observation, it was found:

1. The coanda effect and attachment length are functions of inlet and outlet diameter, length of flow, and distance to the nearest wall;

2. The inlet located in the middle of the inlet wall results in bi-stable flows when D_1/L is small enough to permit attachment;

3. Flow patterns are independent of Reynolds number above a threshold value (approx. 3,800).

Conclusions based on evaluations of the numerical results obtained from the numerical model are:

1. A simple numerical (inviscid) model can be used to predict flow patterns and velocity fields for flows in which the vorticity is produced primarily at the inlet; however, the inviscid approximation does lead to errors in velocity predictions near fixed walls;

2. The vorticity produced along the walls (other than at the inlet) has a small effect upon the internal flow patterns;

3. A 21 x 21 grid is adequate to describe the flow region for the numerical model;

4. Small perturbations (10%) in eddy vorticity cause a jet to deflect from an unstable location;

5. Initial conditions do not affect the flow patterns predicted;

6. The predicted attachment length is a function of inlet diameter and length of flow.

Results from the numerical model, a kinematic relation, suggests that the following additional conclusions can be made concerning the dynamics of the flow:

1. Vorticity in a standing eddy is constant and uniform;

2. The maximum tangential velocity of the standing eddies dictates the magnitude of the vorticity in the standing eddies;

3. The use of the average magnitude of the maximum jet vorticity along the entire length is reasonable based upon comparison of predicted and photographed flow patterns.

APPENDIX A

The tangential velocity of a standing eddy, u_e, is related to the velocity of the jet by applying the circulation theorem (Sabersky [17]).

$$\oint u \, ds = \iint \omega \cdot dA \qquad A.1$$

Applying Eq A.1 to the geometry depicted by Fig. A-1, first to the inner core

$$2u_e \pi r = \omega A = \omega \pi r^2 \qquad A.2$$

Now, apply Eq A.1 to the outer cylinder

$$u_{jet}(1-\sigma)2\pi r = \{\omega_{jet}(1-\sigma) + \sigma(\omega_e)\}(\pi r^2 - \pi r'^2) + \pi r^2 \omega_e \qquad A.3$$

If a thin boundary layer is assumed, r approaches r', and Eq A.3 reduces to

$$u_{jet}(1-\sigma)2\pi r = \pi r^2 \omega_e \qquad A.4$$

Simplifying Eq A.4

$$2u_{jet}(1-\sigma) = \omega_e r \qquad A.5$$

If Eq A.2 is divided by Eq A.5, the needed relationship is obtained

$$\frac{u_e}{u_{jet}} = (1-\sigma) \qquad A.6$$

NOMENCLATURE

B_1 distance from bottom of inlet to bottom wall

B_2 distance from bottom of outlet to bottom wall

b mixing layer thickness between jet and standing eddy (used to calculate jet vorticity in numerical model)

c contraction ratio

D_1 inlet width

D_2 outlet width

H heigh of chamber

k number of filtering screens

L length of chamber

l_r distance for jet to attach to a wall

Q mass flow rate in jet

Q_o mass flow rate through chamber

r radius of core (solid body) in rotation

t time

u velocity in x direction

u_e maximum tangential velocity in a standing eddy

u_{jet} velocity of jet at centerline (y=0)

V tangential velocity of a solid body in rotation

v velocity in y direction

X_H length of initial region of a free jet

y_e value of y corresponding to u_e in jet velocity profile

Z depth of chamber, z dimension

Greek Symbols

α_1 angle at which jet diverges in initial region

α_2 angle at which jet diverges in main region

σ_o thickness of jet boundary layer at x=0

Δu velocity difference between centerline of jet and standing eddy

ΔV velocity difference in a free jet profile

ΔV_m maximum velocity difference in free jet profile

ν kinematic viscosity

σ ratio of the fixed length to the perimeter of a standing eddy

ψ Stokes stream function

ψ_n defines break points in vorticity distribution n=1 to 5

ω vorticity

ω_{jet} maximum magnitude of vorticity in a free jet profile

Subscripts

B bottom

e refers to standing eddy

jet refers to jet

o value of a variable at x=0

T top

x value of a variable at location x

REFERENCES

1. ASAE Yearbook. St. Joseph, Michigan, 1978.

2. ASHRAE Handbook and Product Directory: Fundamentals 1977. ASHRAE, Inc., New York, N.Y. 1977.

3. Reynolds, O., "On the Dynamical Theory of Imcompressible Viscous Fluids and the Determination of the Criterion," Philosophical Transactions of the Royal Society of London, Series A, 186:123, 1895.

4. Taylor, G. I., "Statistical Theory of Turbulence," Proceedings of the Royal Society of London, Series A, 151:421, 1935.

5. Von Karman, T., "The Fundamentals of the Statistical Theory of Turbulence," J. Aeronauti Science, 4:131, 1937.

6. Launder, B. E. and Spalding, D. B., Mathematical Models of Turbulence. Academic Press, N.Y., 1972.

7. Lumley, J. L., "Computational Modelling of Turbulene Flows," Submitted to Advances in App Mechanics. 1978a.

8. Parczewski, K. I. and Renzi, P. N., "Scale Model Studies of Temperature Distribution in Internally Heated Enclosures," ASHRAE Transactions, 69:453-463, 1963.

9. Reinmann, J. J., Koested, A., and Tuve, G. E., "Evaluation of Three Room Air Distributio System for Summer Cooling," ASHRAE Transactions, 65:717-734, 1959.

10. Lumley, John L. A private communication, Cornell Univ., 1978.

11. Dryden, H. L. and Schubauer, G. B., "The Use of Damping Screens for the Reduction of Winc Tunnel Turbulence," J. Aeronautical Science, April, 1947.

12. Foerthmann, E., "Turbulent Jet Expansion," NACA TM 789, 1934.

13. Timmons, Michael B., Experimental and Numerical Study of Air Movement in Slot-Ventilated Enclosures. Ph.D. Thesis, Cornell Univ., 1979.

14. Roache, P. J., Computational Fluid Dynamics. Hermosa Publishers, Albuquerque, N.M., 197

15. Abramovich, G. N., The Theory of Turbulent Jets. M.I.T. Press, Mass. Institute of Technol Cambridge, Mass., 1963.

16. Albertson, J. L., Dai, Y. B., Jensen, R. A., and Rouse, H., "Diffusion of Submerged Jets Proceedings ASCE, 74:1751, 1948.

17. Sabersky, R. H. and Acosta, A. J., Fluid Flow. McMillan Co., N.Y., 1964.

18. Squire, H. B., "Note on the Motion Inside a Region of Recirculation (Cavity Flow)," J. Ro Aeronautical Society. March, pg. 203, 1956.

19. Borque, C. and Newman, B. G., "Reattachment of a Two-dimensional Imcompressible Jet to ar Adjacent Flat Plate," The Aeronautical Quarterly, XI (Aug.): 201, 1960.

20. Sawyer, R. A., "The Flow Due to a Two-dimensional Jet Issuing Parallel to a Flat Plate," Journal Fluid Mechanics, 9(4):543, 1960.

21. Tennekes, H. and Lumley, J. L., A First Course in Turbulence, M.I.T. Press, Cambridge, 1

22. Tani, Itiro (Gortler, H. editor). "Experimental Investigation of Flow Separation Over a Step," International Union of Theoretical and Applied Mechanics. Boundary Layer Researc Symposium, Freiburgg/Br. August, 1957.

TABLE 2 (cont'd.)

21	0.000	0.010	0.066	0.173	0.334	0.533	0.750	0.962	1.158	1.339	1.504	1.656	1.794	1.919	2.033	2.135	2.227	2.309	2.382	2.447	2.502
	2.550	2.588	2.618	2.638	2.650	2.651	2.642	2.622	2.591	2.547	2.489	2.416	2.325	2.216	2.085	1.930	1.747	1.534	1.286	1.000	
22	0.000	0.007	0.061	0.164	0.320	0.516	0.732	0.943	1.136	1.318	1.483	1.633	1.771	1.896	2.009	2.112	2.205	2.288	2.362	2.428	2.486
	2.534	2.575	2.606	2.628	2.641	2.643	2.635	2.616	2.586	2.542	2.484	2.412	2.322	2.213	2.082	1.928	1.746	1.533	1.286	1.000	
23	0.000	0.004	0.053	0.152	0.303	0.495	0.707	0.918	1.112	1.290	1.454	1.604	1.740	1.865	1.978	2.081	2.174	2.258	2.334	2.401	2.460
	2.511	2.553	2.586	2.610	2.624	2.627	2.621	2.603	2.573	2.530	2.473	2.401	2.312	2.205	2.075	1.922	1.741	1.530	1.284	1.000	
24	0.000	-0.000	0.044	0.137	0.282	0.468	0.676	0.886	1.076	1.256	1.418	1.567	1.702	1.826	1.939	2.041	2.135	2.220	2.297	2.366	2.426
	2.479	2.523	2.558	2.583	2.598	2.604	2.598	2.581	2.552	2.511	2.455	2.385	2.297	2.191	2.064	1.912	1.734	1.525	1.282	1.000	
25	0.000	-0.005	0.034	0.120	0.257	0.436	0.639	0.847	1.036	1.214	1.375	1.522	1.657	1.779	1.891	1.994	2.087	2.173	2.251	2.322	2.384
	2.438	2.484	2.521	2.549	2.565	2.572	2.568	2.552	2.525	2.484	2.431	2.362	2.276	2.172	2.047	1.899	1.723	1.518	1.278	1.000	
26	0.000	-0.011	0.023	0.102	0.230	0.400	0.597	0.801	0.991	1.166	1.325	1.471	1.603	1.724	1.835	1.937	2.031	2.118	2.197	2.269	2.333
	2.389	2.437	2.476	2.505	2.524	2.532	2.529	2.515	2.489	2.451	2.399	2.332	2.249	2.148	2.026	1.881	1.710	1.509	1.273	1.000	
27	0.000	-0.016	0.011	0.082	0.200	0.361	0.550	0.748	0.938	1.111	1.268	1.411	1.542	1.662	1.771	1.873	1.966	2.053	2.134	2.207	2.273
	2.332	2.382	2.423	2.454	2.475	2.485	2.483	2.471	2.447	2.410	2.360	2.296	2.216	2.118	2.000	1.860	1.693	1.497	1.268	1.000	
28	0.000	-0.022	-0.002	0.061	0.168	0.319	0.498	0.691	0.879	1.048	1.203	1.344	1.473	1.590	1.699	1.799	1.893	1.980	2.061	2.137	2.205
	2.266	2.318	2.362	2.395	2.417	2.429	2.430	2.419	2.396	2.362	2.315	2.255	2.177	2.083	1.970	1.834	1.673	1.484	1.261	1.000	
29	0.000	-0.028	-0.015	0.040	0.136	0.275	0.444	0.628	0.811	0.979	1.132	1.270	1.396	1.511	1.617	1.717	1.810	1.898	1.980	2.057	2.128
	2.191	2.247	2.292	2.328	2.352	2.366	2.368	2.359	2.339	2.306	2.262	2.204	2.131	2.042	1.934	1.804	1.650	1.468	1.253	1.000	
30	0.000	-0.034	-0.027	0.019	0.105	0.230	0.387	0.561	0.738	0.904	1.053	1.188	1.311	1.423	1.527	1.625	1.717	1.806	1.890	1.969	2.042
	2.108	2.166	2.215	2.253	2.280	2.295	2.299	2.292	2.273	2.243	2.202	2.147	2.079	1.995	1.892	1.770	1.623	1.449	1.243	1.000	
31	0.000	-0.040	-0.039	-0.000	0.075	0.186	0.330	0.492	0.660	0.821	0.967	1.099	1.218	1.327	1.428	1.524	1.616	1.704	1.790	1.871	1.947
	2.017	2.078	2.129	2.170	2.199	2.216	2.222	2.216	2.200	2.173	2.134	2.084	2.020	1.941	1.846	1.731	1.593	1.428	1.233	1.000	
32	0.000	-0.044	-0.050	-0.019	0.046	0.144	0.273	0.422	0.579	0.733	0.875	1.002	1.117	1.222	1.320	1.413	1.504	1.593	1.680	1.764	1.844
	1.917	1.981	2.036	2.079	2.110	2.129	2.136	2.133	2.119	2.094	2.059	2.013	1.954	1.882	1.793	1.687	1.558	1.405	1.220	1.000	
33	0.000	-0.048	-0.059	-0.035	0.020	0.105	0.218	0.352	0.496	0.639	0.775	0.897	1.007	1.108	1.202	1.293	1.382	1.472	1.561	1.648	1.731
	1.808	1.877	1.935	1.981	2.015	2.035	2.043	2.041	2.029	2.008	1.976	1.934	1.881	1.819	1.735	1.637	1.520	1.378	1.207	1.000	
34	0.000	-0.051	-0.066	-0.049	-0.003	0.070	0.167	0.284	0.413	0.544	0.669	0.785	0.889	0.985	1.074	1.162	1.249	1.340	1.431	1.522	1.609
	1.690	1.764	1.826	1.876	1.911	1.932	1.943	1.942	1.932	1.913	1.885	1.848	1.801	1.742	1.670	1.582	1.476	1.348	1.191	1.000	
35	0.000	-0.053	-0.071	-0.059	-0.021	0.039	0.120	0.221	0.332	0.448	0.560	0.666	0.763	0.853	0.937	1.020	1.105	1.197	1.292	1.386	1.478
	1.565	1.643	1.710	1.764	1.801	1.823	1.834	1.834	1.826	1.810	1.786	1.754	1.713	1.661	1.598	1.522	1.428	1.314	1.174	1.000	
36	0.000	-0.053	-0.072	-0.065	-0.035	0.014	0.081	0.162	0.255	0.354	0.452	0.544	0.630	0.711	0.788	0.867	0.950	1.042	1.141	1.241	1.338
	1.430	1.514	1.587	1.644	1.683	1.706	1.716	1.718	1.712	1.698	1.678	1.651	1.616	1.573	1.520	1.454	1.374	1.276	1.154	1.000	
37	0.000	-0.050	-0.070	-0.066	-0.043	-0.005	0.048	0.112	0.186	0.265	0.345	0.422	0.495	0.563	0.631	0.701	0.780	0.876	0.979	1.085	1.188
	1.287	1.377	1.457	1.520	1.559	1.581	1.591	1.593	1.588	1.578	1.562	1.540	1.512	1.477	1.433	1.380	1.315	1.234	1.132	1.000	
38	0.000	-0.045	-0.062	-0.061	-0.045	-0.016	0.022	0.070	0.125	0.184	0.245	0.304	0.360	0.414	0.468	0.527	0.599	0.697	0.807	0.919	1.030
	1.135	1.233	1.321	1.390	1.438	1.448	1.457	1.459	1.456	1.448	1.436	1.419	1.398	1.372	1.339	1.298	1.248	1.186	1.106	1.000	
39	0.000	-0.036	-0.049	-0.049	-0.039	-0.020	0.005	0.037	0.073	0.112	0.152	0.192	0.231	0.268	0.306	0.348	0.407	0.508	0.624	0.743	0.861
	0.974	1.061	1.176	1.257	1.292	1.307	1.314	1.316	1.314	1.309	1.301	1.290	1.275	1.257	1.235	1.208	1.174	1.132	1.077	1.000	
40	0.000	-0.021	-0.029	-0.029	-0.024	-0.015	-0.002	0.013	0.031	0.051	0.071	0.091	0.110	0.128	0.148	0.171	0.208	0.315	0.436	0.560	0.683
	0.804	0.920	1.030	1.125	1.149	1.158	1.162	1.163	1.162	1.159	1.155	1.150	1.143	1.134	1.123	1.109	1.092	1.070	1.042	1.000	
41	0.000	0.000	0.000	0.000	0.000	0.000	0.000	0.000	0.000	0.000	0.000	0.000	0.000	0.000	0.000	0.000	0.000	0.000	0.125	0.250	0.375	0.500
	0.625	0.750	0.875	1.000	1.000	1.000	1.000	1.000	1.000	1.000	1.000	1.000	1.000	1.000	1.000	1.000	1.000	1.000	1.000	1.000	

TABLE 3

Numerical Fields of Stream Function for Test 2

1	0.000	0.000	0.000	0.000	0.000	0.000	0.000	0.000	0.000	0.000	0.000	0.000	0.000	0.000	0.000	0.000	0.000	0.000	0.000	0.000	0.000
2	0.000	-0.013	-0.026	-0.002	0.004	0.010	0.014	0.017	0.018	0.016	0.013	0.005	0.003	-0.004	-0.010	-0.012	-0.020	-0.027	-0.031	-0.031	-0.023	0.000
3	0.000	-0.000	0.012	0.027	0.041	0.053	0.062	0.068	0.069	0.067	0.061	0.052	0.039	0.024	0.008	-0.008	-0.016	-0.023	-0.034	-0.038	-0.029	0.000
4	0.000	0.030	0.062	0.090	0.114	0.133	0.147	0.155	0.158	0.154	0.145	0.130	0.110	0.087	0.061	0.035	0.009	-0.011	-0.024	-0.023	-0.006	0.000
5	0.000	0.092	0.147	0.189	0.223	0.250	0.269	0.281	0.284	0.279	0.266	0.245	0.218	0.185	0.147	0.108	0.070	0.035	0.008	-0.006	0.000	
6	0.167	0.223	0.279	0.330	0.373	0.406	0.433	0.448	0.452	0.446	0.429	0.401	0.364	0.319	0.267	0.214	0.160	0.107	0.053	0.022	0.000	
7	0.333	0.388	0.446	0.503	0.552	0.590	0.617	0.633	0.638	0.631	0.613	0.582	0.540	0.486	0.423	0.353	0.280	0.207	0.136	0.065	0.000	
8	0.500	0.566	0.628	0.684	0.732	0.769	0.795	0.810	0.815	0.809	0.792	0.763	0.721	0.665	0.597	0.519	0.432	0.339	0.242	0.138	0.000	
9	0.667	0.737	0.795	0.846	0.890	0.925	0.950	0.966	0.971	0.966	0.950	0.922	0.883	0.831	0.767	0.690	0.600	0.498	0.389	0.276	0.167	
10	0.833	0.886	0.936	0.982	1.024	1.058	1.083	1.099	1.105	1.101	1.086	1.061	1.025	0.977	0.918	0.847	0.763	0.666	0.558	0.443	0.333	
11	1.000	1.007	1.047	1.092	1.133	1.167	1.193	1.210	1.217	1.214	1.201	1.178	1.145	1.102	1.048	0.983	0.907	0.821	0.724	0.615	0.500	
12	1.000	1.063	1.120	1.172	1.216	1.252	1.280	1.297	1.306	1.304	1.294	1.274	1.244	1.205	1.156	1.098	1.030	0.953	0.866	0.774	0.667	
13	1.000	1.092	1.166	1.227	1.276	1.314	1.343	1.362	1.371	1.372	1.363	1.346	1.320	1.285	1.241	1.189	1.129	1.062	0.989	0.911	0.833	
14	1.000	1.109	1.194	1.261	1.313	1.354	1.384	1.403	1.414	1.416	1.409	1.395	1.372	1.341	1.302	1.256	1.202	1.143	1.081	1.024	1.000	
15	1.000	1.116	1.206	1.276	1.331	1.372	1.402	1.422	1.433	1.436	1.431	1.419	1.399	1.372	1.339	1.297	1.249	1.195	1.135	1.076	1.000	
16	1.000	1.116	1.206	1.276	1.329	1.368	1.397	1.416	1.427	1.431	1.429	1.418	1.401	1.379	1.349	1.314	1.271	1.221	1.160	1.089	1.000	
17	1.000	1.110	1.195	1.259	1.307	1.343	1.369	1.387	1.397	1.401	1.398	1.391	1.378	1.359	1.335	1.304	1.267	1.221	1.165	1.093	1.000	
18	1.000	1.098	1.171	1.226	1.266	1.296	1.317	1.332	1.340	1.344	1.342	1.337	1.327	1.312	1.293	1.269	1.239	1.201	1.152	1.087	1.000	
19	1.000	1.078	1.133	1.174	1.203	1.225	1.240	1.250	1.256	1.259	1.259	1.256	1.248	1.238	1.225	1.206	1.186	1.159	1.122	1.071	1.000	
20	1.000	1.047	1.078	1.100	1.116	1.127	1.135	1.140	1.143	1.145	1.145	1.143	1.139	1.134	1.128	1.119	1.108	1.093	1.073	1.044	1.000	
21	1.000	1.000	1.000	1.000	1.000	1.000	1.000	1.000	1.000	1.000	1.000	1.000	1.000	1.000	1.000	1.000	1.000	1.000	1.000	1.000	1.000	

TABLE 4

Numerical Fields of Stream Function for Test 3

1	0.000	0.000	0.000	0.000	0.000	0.167	0.333	0.500	0.667	0.833	1.000	1.000	1.000	1.000	1.000	1.000	1.000	1.000	1.000	1.000	1.000
2	0.000	0.014	0.042	0.091	0.165	0.278	0.415	0.561	0.703	0.830	0.933	0.998	1.040	1.067	1.082	1.089	1.088	1.080	1.063	1.038	1.000
3	0.000	0.031	0.081	0.149	0.240	0.354	0.484	0.618	0.746	0.857	0.949	1.020	1.073	1.110	1.132	1.141	1.138	1.124	1.096	1.056	1.000
4	0.000	0.045	0.108	0.185	0.290	0.409	0.536	0.666	0.787	0.891	0.979	1.050	1.104	1.142	1.166	1.175	1.169	1.149	1.115	1.065	1.000
5	0.000	0.055	0.127	0.217	0.327	0.451	0.582	0.709	0.824	0.924	1.008	1.077	1.130	1.168	1.190	1.197	1.189	1.166	1.126	1.071	1.000
6	0.000	0.062	0.141	0.238	0.354	0.482	0.614	0.741	0.853	0.950	1.033	1.100	1.151	1.187	1.208	1.213	1.203	1.176	1.134	1.075	1.000
7	0.000	0.067	0.151	0.253	0.373	0.504	0.637	0.763	0.874	0.970	1.051	1.116	1.166	1.201	1.220	1.224	1.212	1.183	1.139	1.078	1.000
8	0.000	0.070	0.157	0.262	0.385	0.517	0.651	0.776	0.886	0.982	1.062	1.126	1.176	1.210	1.228	1.230	1.217	1.187	1.142	1.079	1.000
9	0.000	0.071	0.159	0.265	0.389	0.523	0.657	0.782	0.891	0.986	1.066	1.130	1.179	1.213	1.231	1.233	1.219	1.189	1.143	1.080	1.000
10	0.000	0.072	0.158	0.264	0.387	0.520	0.654	0.779	0.889	0.984	1.064	1.128	1.178	1.211	1.230	1.232	1.218	1.188	1.142	1.080	1.000
11	0.000	0.069	0.153	0.257	0.378	0.510	0.643	0.766	0.879	0.974	1.055	1.120	1.170	1.205	1.224	1.227	1.215	1.186	1.140	1.079	1.000
12	0.000	0.064	0.145	0.244	0.362	0.491	0.623	0.749	0.860	0.957	1.038	1.105	1.157	1.193	1.214	1.219	1.208	1.181	1.137	1.077	1.000
13	0.000	0.056	0.134	0.227	0.339	0.464	0.594	0.719	0.832	0.931	1.015	1.084	1.138	1.176	1.199	1.207	1.198	1.173	1.132	1.074	1.000
14	0.000	0.051	0.119	0.205	0.309	0.428	0.555	0.680	0.795	0.896	0.983	1.055	1.112	1.154	1.180	1.190	1.185	1.163	1.126	1.071	1.000
15	0.000	0.042	0.101	0.177	0.272	0.383	0.505	0.630	0.748	0.852	0.943	1.018	1.079	1.125	1.156	1.170	1.165	1.151	1.116	1.067	1.000
16	0.000	0.031	0.080	0.145	0.229	0.331	0.446	0.568	0.687	0.797	0.892	0.974	1.040	1.091	1.127	1.146	1.150	1.137	1.108	1.062	1.000
17	0.000	0.020	0.057	0.111	0.182	0.271	0.378	0.494	0.614	0.730	0.832	0.921	0.994	1.052	1.093	1.119	1.128	1.121	1.097	1.057	1.000
18	0.000	0.004	0.033	0.079	0.132	0.208	0.301	0.411	0.529	0.649	0.762	0.860	0.943	1.009	1.058	1.089	1.104	1.103	1.085	1.051	1.000
19	0.000	-0.001	0.009	0.037	0.080	0.140	0.217	0.315	0.431	0.556	0.680	0.793	0.890	0.967	1.023	1.059	1.078	1.082	1.070	1.043	1.000
20	0.000	-0.013	-0.007	0.007	0.031	0.065	0.122	0.199	0.314	0.450	0.592	0.728	0.847	0.941	0.998	1.031	1.048	1.053	1.047	1.030	1.000
21	0.000	0.000	0.000	0.000	0.000	0.000	0.000	0.000	0.167	0.333	0.500	0.667	0.833	1.000	1.000	1.000	1.000	1.000	1.000	1.000	1.000

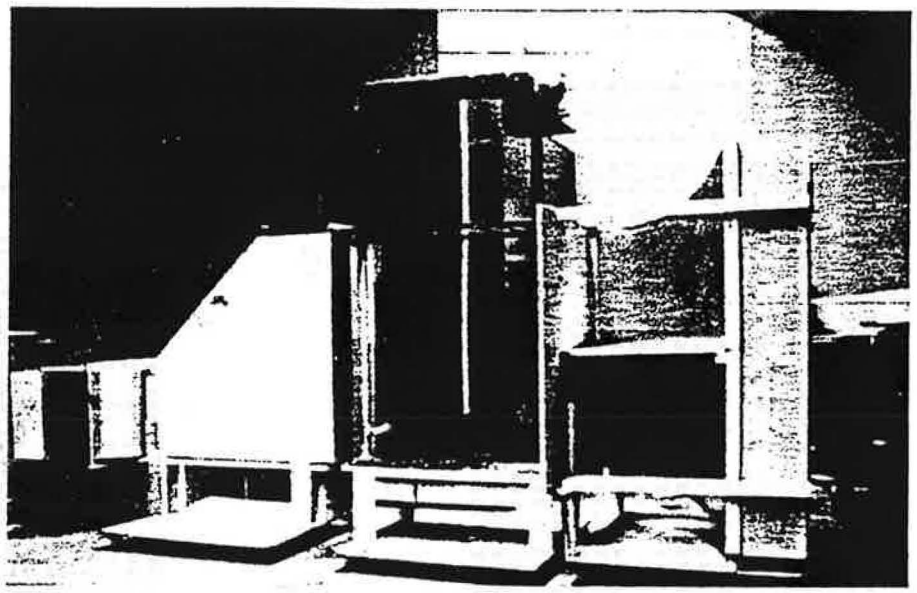

Fig. 1 Wind tunnel used to obtain flow patterns and velocity data

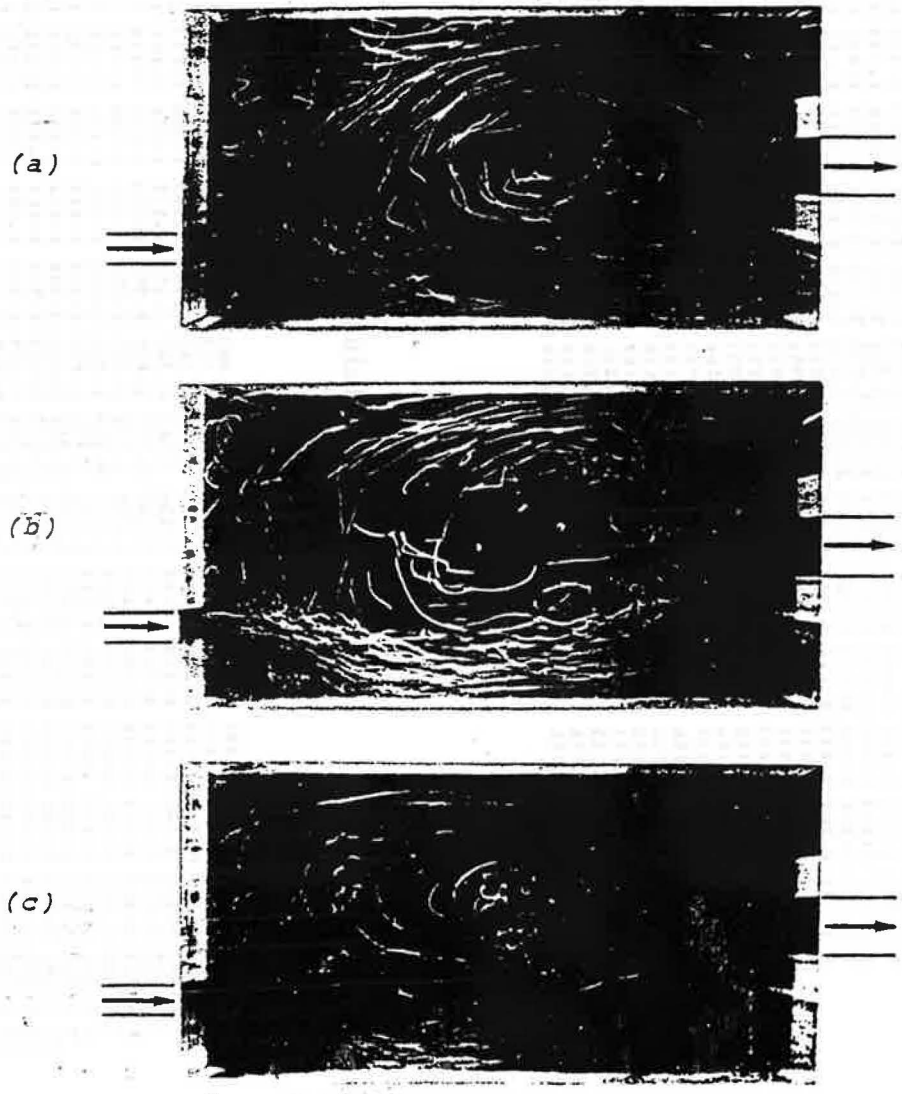

F Comparison of flow patterns at three Reynolds numbers: 3,800 (a), b) and 11,000 (c) (arrows identify air inlet and outlet)

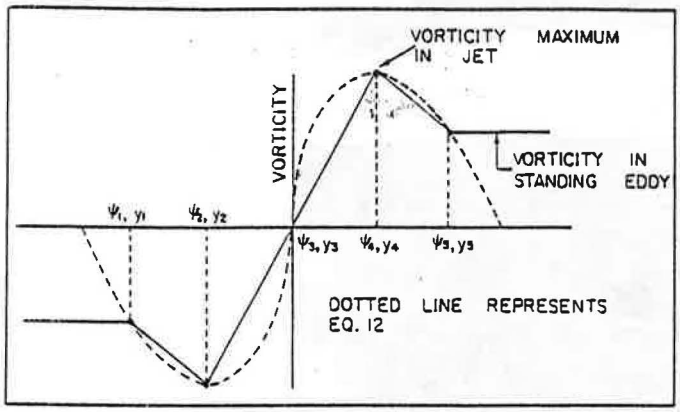

Fig. 3 Approximation used for the vorticity profile of a jet with standing eddies above and below the jet

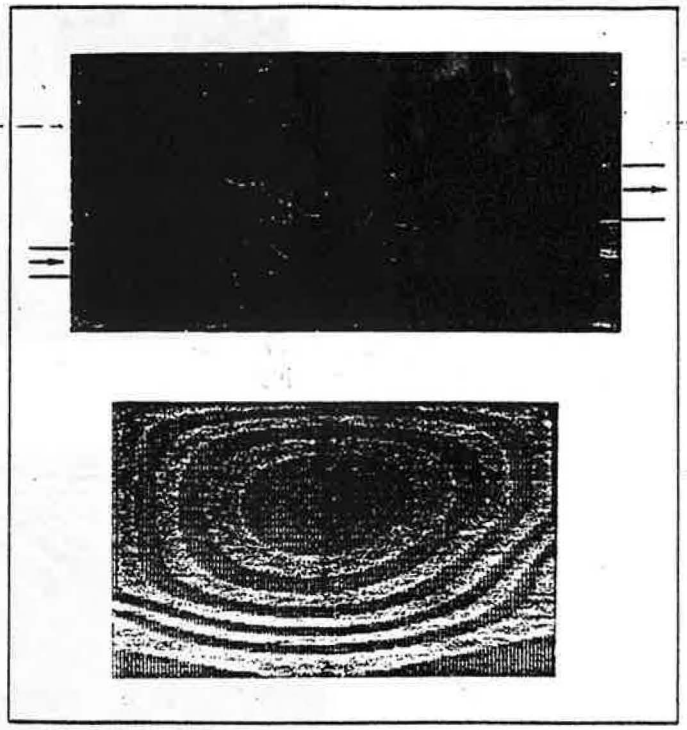

Fig. 4 A comparison between predicted and photographed flow patterns for geometry specified in Table 1 as Test 1

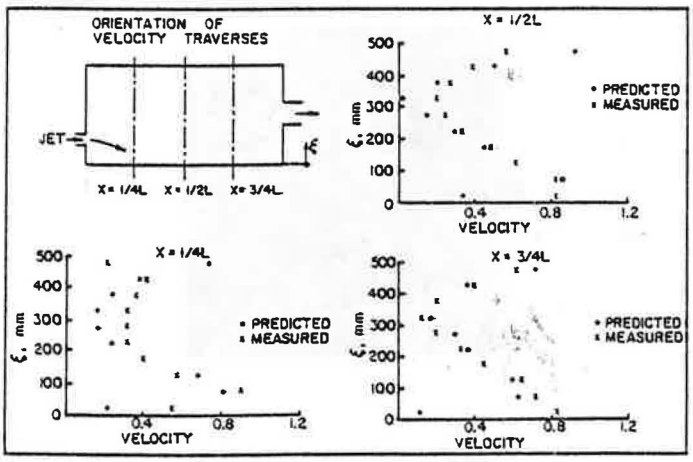

Fig. 5 A comparison between predicted and measured velocities for geometry specified in Table 1 as Test 1

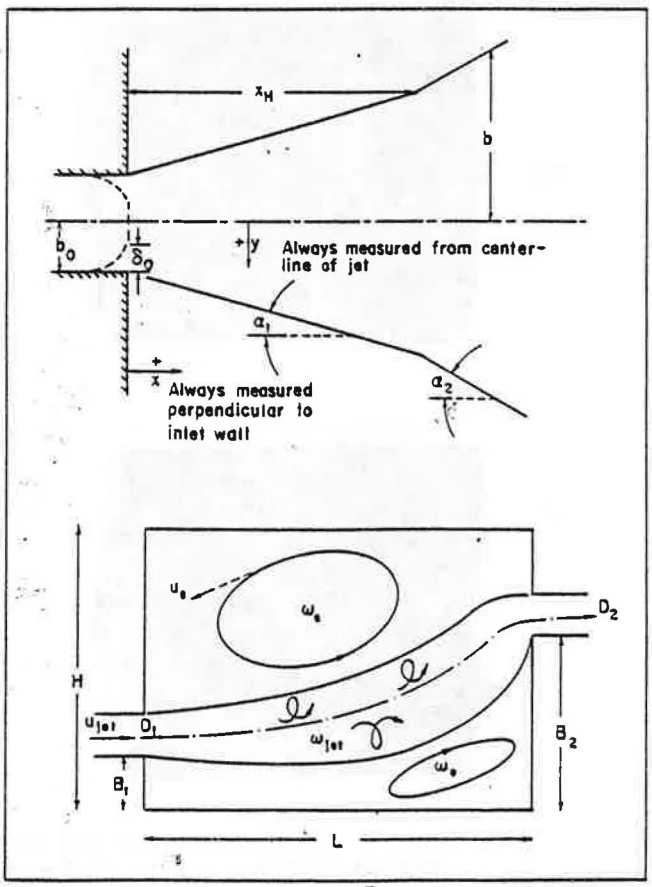

Fig. 6 Variables used to describe enclosure geometry and coordinate location for a free jet and a recirculating flow

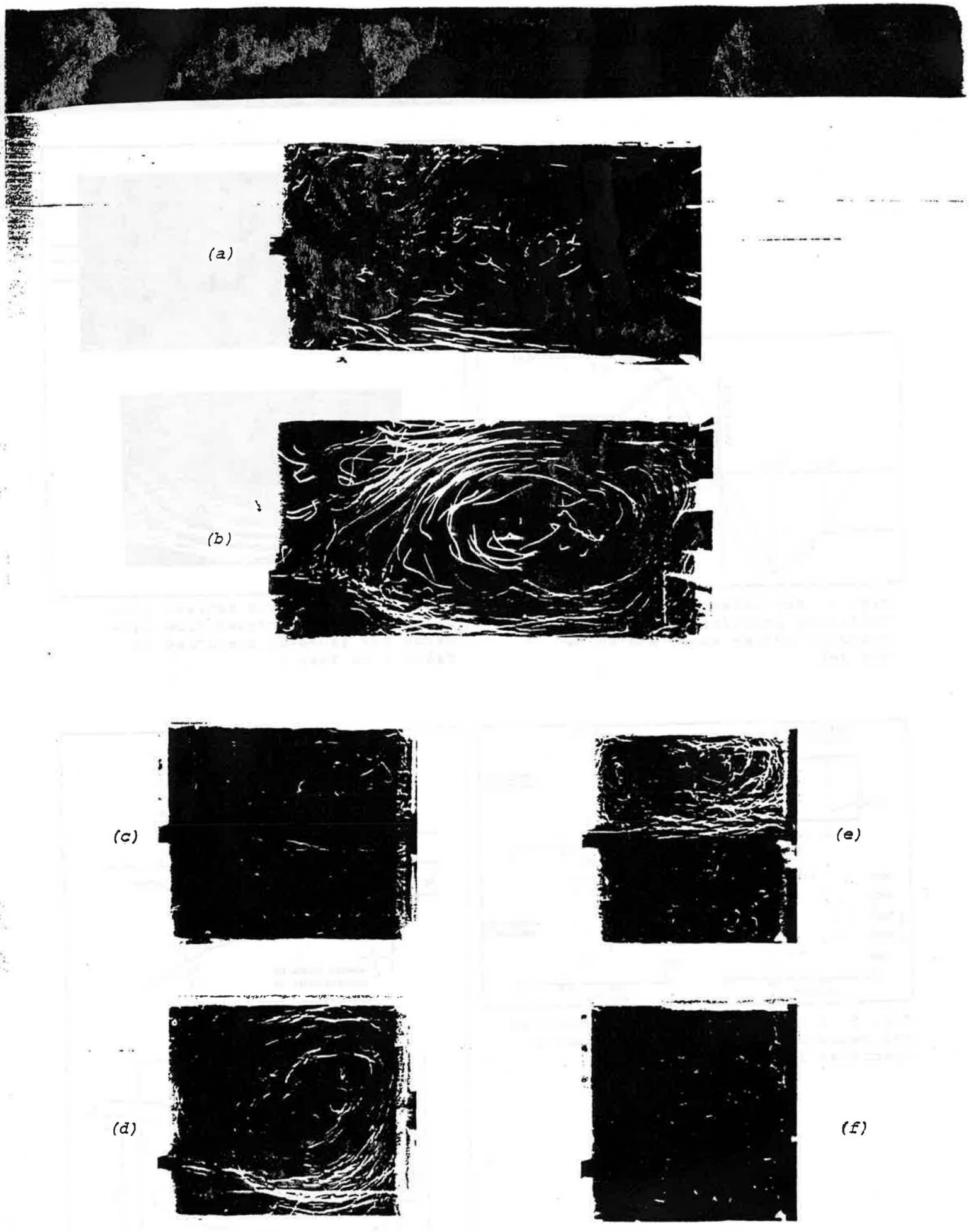

Fig. 7 Disappearance of the coanda effect as the enclosure lenghth shortens and/or distance from the bottom of the inlet to wall increases (L = 1,000 mm, B_1 = 100 (a) or 225 mm (b) - top photographs; L = 600 mm, B_1 = 100 (c) or 225 mm (d) - lower left photographs; L = 500 mm, B_1 = 100 (e) or 225 mm (f) - lower right photographs)